

Journal Pre-proofs

Research papers

The potential impact of climate variability on siltation of Andean reservoirs

Miluska A. Rosas, Veerle Vanacker, Willem Viveen, Ronald R. Gutierrez,
Christian Huggel

PII: S0022-1694(19)31131-X
DOI: <https://doi.org/10.1016/j.jhydrol.2019.124396>
Reference: HYDROL 124396

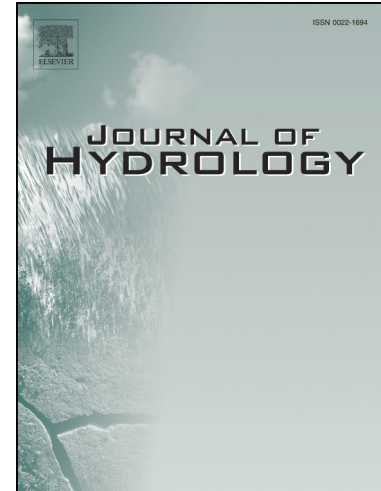
To appear in: *Journal of Hydrology*

Received Date: 22 March 2019
Revised Date: 23 October 2019
Accepted Date: 22 November 2019

Please cite this article as: Rosas, M.A., Vanacker, V., Viveen, W., Gutierrez, R.R., Huggel, C., The potential impact of climate variability on siltation of Andean reservoirs, *Journal of Hydrology* (2019), doi: <https://doi.org/10.1016/j.jhydrol.2019.124396>

This is a PDF file of an article that has undergone enhancements after acceptance, such as the addition of a cover page and metadata, and formatting for readability, but it is not yet the definitive version of record. This version will undergo additional copyediting, typesetting and review before it is published in its final form, but we are providing this version to give early visibility of the article. Please note that, during the production process, errors may be discovered which could affect the content, and all legal disclaimers that apply to the journal pertain.

© 2019 Published by Elsevier B.V.



The potential impact of climate variability on siltation of Andean reservoirs

Miluska A. Rosas^{a,b,*}, Veerle Vanacker^a, Willem Viveen^b, Ronald R. Gutierrez^{b,c}, Christian Huggel^d

^a Earth and Life Institute, Georges Lemaître Centre for Earth and Climate Research, Université catholique de Louvain, Belgium.

^b Grupo de Investigación en Geología Sedimentaria, Especialidad de Ingeniería Geológica, Departamento de Ingeniería, Pontificia Universidad Católica del Perú. Av. Universitaria 1801, San Miguel, Lima, Perú.

^c Universidad del Norte, Barranquilla, Colombia

^d Department of Geography, University of Zurich, Switzerland

*Corresponding author. Email address: miluska.rosas@pucp.pe

Abstract

Recent changes in global climate, and especially changes in precipitation patterns, may negatively impact on siltation of Andean storage reservoirs, thereby putting at risk the provision of resources to the local population. The extent to which this may happen is poorly understood. We therefore studied the catchment of the Cañete River in the western Peruvian Coastal Range as it plays an important role in the socioeconomic development of the region. It houses the 220MW El Platanal hydroelectric plant and the Capillucas reservoir that provide the surrounding areas with water and energy. We used a hydrological model (HEC-HMS) coupled with a sediment transport model (HEC-RAS) to simulate future changes in river discharge and sediment load. This information was then used to calculate the siltation of the Capillucas storage reservoir. Ten scenarios were developed, a combination of two different precipitation patterns and five different precipitation rates. The precipitation patterns differed in the distribution of the precipitation change during the rainfall season, and the precipitation rates differed in the extent of change in precipitation amounts. The average sediment load of the Cañete River was estimated at 981 kTon/yr upstream of the Capillucas reservoir and showed that the calculated life span of the Capillucas reservoir is about 17 years. The most pessimistic scenario suggested a reduction in the life span of the reservoir to 7 years and the most optimistic scenario to 31 years. Even under the most optimistic scenario, the life span of the reservoir is shorter than its officially expected functionality of 50 years. As such, our results demonstrated the vulnerability of Andean hydroelectric reservoirs against future climate change.

Keywords

Erosion; Sediment transport; Climate change; Andes; Hydroelectric projects; Storage dams

1. Introduction

The global water storage capacity of hydroelectric reservoirs is decreasing annually while the economic activity, the hydropower industry and the world population continue to grow strongly (Palmieri et al., 2003). Therefore, sustainable management of reservoirs and water resource infrastructure is necessary to guarantee the projected usable lifespan of the hydroelectric infrastructure for future generations. About 80% of the reservoir volume in Europe will be filled up with sediments by the year 2080, and in North America by the year 2060 (Hauer et al., 2018). Likewise, in the near future, the hydropower sector will be impacted by an increase in sediment production due to global warming (Hauer et al., 2018). Large dams interrupt water flow and sediment transport, and trigger deposition of sediments in the middle or lower reaches of rivers as well as inundations of the surrounding areas. Sedimentation in the reservoirs might add compressional forces on the dam structure thereby exceeding the normal hydrostatic design, and the decrease of water storage in the reservoir and clogging of water intake also hinders the production of energy (Morris et al., 2008; Annandale, 2016). In this sense, the World Bank proposed a life cycle management approach for reservoir infrastructure with special emphasis on the economic evaluation of sediment management (Palmieri et al., 2003). It highlighted techniques to reduce the influx of sediments, to manage and evacuate sediments from the reservoir, and to replace lost storage of the reservoirs.

The boom in hydropower development in Andean river basins was identified as one of the top 15 global conservation issues (Sutherland et al., 2013). For this region, the electricity generation might increase by 550% from 2005 to the year 2050, thereby needing an increase in water volume from 70.5 billion m³ to 150.7 billion m³ (WEC, 2010). Of the Andean countries, Peru has the highest numbers of existing and proposed hydropower projects, because of its rapidly evolving energy demands (estimated at 8% growth per year) and regulatory framework

that aims at promoting renewable energy (Tamayo et al., 2016; World Bank, 2017). Existing studies on the sustainability of its reservoirs are mainly focused on the largest ones, for example the Gallito Ciego and Poechos reservoirs in north western Peru. The admissible sediments storage limit (dead storage) in Gallito Ciego reservoir was reached in 10 years, even though its designed lifespan was 50 years (Ramírez and Cisneros, 2007). The Poechos reservoir was highly affected by recent El Niño events where the average sediment fluxes exceeded those of normal years by a factor of 11 thereby shortening its life span considerably (Tote et al., 2011).

Despite these initial efforts, studies that describe the impact of changing sediment transfer due to climate change to the hydroelectric infrastructural system are still limited (Latrubesse and Restrepo, 2014). This is reason for concern as Andean countries like Peru are highly vulnerable to changes in precipitation rates and precipitation patterns as shown by the recent 2017 and 2018 El Niño Southern Oscillation (ENSO) events (Cadilhac et al., 2017). These high-intensity runoff events are associated with landsliding (Clark et al., 2016), mudflows (Tote et al., 2011), and gully erosion (Molina et al., 2015), and potentially lead to catastrophic flooding downstream (Coppus and Imeson, 2002; Roman-Gonzalez et al., 2019). During such extreme rainfall events the suspended sediment concentrations in Andean rivers may be 360 times higher when compared to normal conditions (Morera et al., 2013).

This paper evaluates the potential impact of climate variability on the water storage capacity of hydroelectric reservoirs in Andean countries, via a case study of the Cañete River in the Peruvian Coastal Range. By using a coupled hydrological-sediment transport model, we assessed projected changes in sediment transport rates under different scenarios of precipitation variability. The model simulations allowed us to evaluate the possible impacts of precipitation change on the life cycle of a hydroelectric plant.

2. Study area: Cañete River basin

2.1 Socioeconomic characteristics

The Cañete River is located approximately 150 km south of Lima (Peru). The basin has an extension of 6,049 km² and connects the Peruvian Andes to the Pacific Ocean (Fig. 1). The lower (Fig. 2b), arid part of the Cañete basin (0-1500 m a.s.l.) is an important agricultural area that produces fig, avocado, lúcuma, orchards, sugar cane, alfalfa crops and river shrimps (INEI, 2017). The middle basin (Fig. 2b) is predominantly sub-humid and hosts subsistence agriculture. The upper part (> 4000 m a.s.l.) is a treeless high-elevation puna landscape where the Nor Yauyos National Park is located. This is an important karst area with extensive limestone caves and upwelling of subterranean ground water. Snow cover and glaciers are present at the headwaters above 5000 m a.s.l. The retreat of glaciers due to global warming is expected to have an impact on water supply downstream the rivers. The change in streamflow seasonality due to a reduction of glacier meltwater will affect water availability and fluvial regimes downstream especially during the dry season (Vuile et al., 2018). In the most optimistic case, future climate change is expected to lead to a 1.6% increase in overall water availability in the Cañete and a 24% decrease in the worst case (Fluixá et al., 2018).

The Cañete basin plays an important role in the socioeconomic development of the region. Approximately 85.2% (2516 hm³) of the surface water resources are destined for energy production and 14.5% (427 hm³) for agriculture. Both of them constitute the prevalent economic activities in the area (ANA, 2017). The Capillucas reservoir, located in the middle section of the basin (Fig. 1), is one of the main operating structures of El Platanal hydropower plant operated by the Peruvian generator Compañía Eléctrica El Platanal S.A (CELEPSA.). The plant has been operational since 2010 and generates up to 220 MWatt of electricity (Tamayo

et al., 2016). The Capillucas dam is 36 m high, 60 m long and located at an elevation of 1543 m a.s.l. Its maximum water storage is $1.4 \times 10^6 \text{ m}^3$ of which $0.8 \times 10^6 \text{ m}^3$ corresponds to the usable capacity. The Cañete basin is highly affected by rapid siltation with sediment delivery from landslides, mud- and debris flows, and gully erosion, principally in the middle and middle-upper reaches of the basin (Fig. 2b). The geomorphic activity is mainly triggered by extreme rainfall events that characterize the area, especially in the headwaters (INDECI, 2012; Rau et al., 2017). In some tributaries the amount of transported sediment in suspension affects periodically the local infrastructure, water quality and local economic activity (INDECI, 2012; 2017; SINAPAD, 2017).

2.2 Physiographic characteristics

The lower Cañete basin is formed in a series of extensional tectonic basins in which over 600 m of sediments have accumulated during the Cenozoic (Viveen and Schlunegger, 2018). The basin lithology presents a large variability of sedimentary, plutonic and volcanic rocks (Fig. 2a). Granites (acid plutonic) cover most of the lower basin coastal range, whereas alluvial fans, debris flows, and ancient flood plains occupy the valley floor. Sedimentary rocks such as sandstones and limestones and intermediate volcanic rocks occur in the middle and middle-upper reaches of the basin. The upper basin reach is made up of carbonate-rich sedimentary rocks such as limestones and dolomites. Above 4500 m a.s.l., glacial landforms and (peri)glacial sediments are present.

The Cañete basin experiences an annual average temperature of 20°C. The rainfall rate in the basin normally ranges from 2.2 mm/day to 44 mm/day but surpasses 70 mm/day during ENSO events (CELEPSA, unpublished data). Within the basin there is a strong topographic control on rainfall patterns, with mean annual precipitation amounts ranging from 20 mm in the lower part of the basin (~721 m a.s.l.) to more than 1000 mm in the upper part of the basin (~4675 m

a.s.l.). Since the 1950s a significant warming was reported for central Peru with a temperature increase of roughly 0.1°C per decade (Vuile et al., 2008). Future temperature projections for the Cañete basin suggest temperature increases ranging from 1°C to 4°C by the end of the 21th century (Fluixá et al., 2018). In contrast to the widely reported warming trend over the Andes, the trends in precipitation are more difficult to predict due to the interannual variability driven by ENSO and the scarcity of long observational meteorological records (Vuile et al., 2018). South American regional climate change models do not provide clear indications of future precipitation change (Marengo et al., 2010; Chou et al., 2014) and large uncertainties remain regarding the long-term trends in precipitation amounts (Vuile et al., 2018). Recently, Fluixá et al. (2018) used downscaling techniques based on GCM-CMIP5 circulation models to address these issues. Their predictions showed large uncertainties in the projected rainfall trends for the Cañete basin with projected changes ranging from -17% to +24% by the end of the 21st century.

3. Materials and methods

A coupled hydrological and sediment transport model was built to simulate water flow and sediment transport in the Cañete River upstream of the Capillucas dam. The HEC-HMS (Arlen, 2000) and HEC-RAS (U.S. Army Corps of Engineering, 2016) platforms were applied to simulate precipitation-runoff and sediment transport. Both models have been widely applied in the USA to describe discharge and sediment transfer in river channels (Knebl et al., 2005; Pereira et al., 2009) and to some extent in data-poor regions (Halwatura and Najim, 2013; Amini et al., 2014).

3.1. Hydrological model

The HEC-HMS platform was developed to simulate precipitation, runoff and hydrologic processes of dendritic basins (Arlen, 2000). It is based on a structure of sub-basins that are interconnected through a channel network and rainfall-runoff generation is calculated

independently for each sub-basin. The model assumes a closed hydrological system, where one part of the precipitation returns to the atmosphere by evapotranspiration, another part infiltrates into the surface, and the remaining part is evacuated by overland flow. Thus, the stream flow is the combination of overland flow, precipitation in water bodies such as lakes and base flow. In the model, baseflow is set to a constant value (Fig. 4), based on the observation of a constant and permanent low flow during the rainy and dry seasons (McCuen, 1989; Coustau, 2012). In the dry seasons, the meltwater of the glaciers located in the headwaters of the Cañete basin provide the base flow.

As a first step, the HEC-HMS platform assigns the observed rainfall data to every sub-basin by applying an inverse distance weighting algorithm (Arlen, 2000). Because the number of meteorological stations is limited, we slightly modified the algorithm to account for the strong correlation between precipitation and altitude in the region (compare to Chang et al., 2005). This modification allows for a better rainfall distribution by reducing the uncertainty related to the limited number of meteorological stations (Eq. 1):

$$P_x = \frac{\sum_{t=1}^n \frac{d_t^j}{(\Delta Z)_t^k} * P_t}{\sum_{t=1}^n \frac{d_t^j}{(\Delta Z)_t^k}} \quad \text{Eq. 1}$$

where d is the distance (m) between the meteorological station i and the evaluated point x ; ΔZ is the elevation difference (m) between i and x ; P is the daily precipitation amount (mm/day); n is the number of meteorological stations; and j and k are geographic parameters.

The HEC-HMS model considers losses through evapotranspiration and infiltration.

Evapotranspiration loss has been estimated by the Turc equation (Eq. 2; (Diouf et al., 2016):

$$ET_0 = a * C * (R_G + b) \frac{T}{T + 15} \quad \text{Eq. 2}$$

where ET_0 is the potential daily evapotranspiration (mm/day); T is the average daily air temperature ($^{\circ}\text{C}$); RG is the global radiation in $\text{MJ}/(\text{m}^2 \cdot \text{day})$ and a , b and C are empirical parameters.

To obtain the accumulative infiltration loss, the initial and constant-rate models have been considered (Arlen, 2000). Here, the precipitation, which is neither retained on the land surface nor infiltrated into the soil, also known as precipitation excess (pe_t), is estimated as the difference between the mean regional precipitation (p_t) and the maximum potential rate of loss (f_c). The regional precipitation is derived from the local meteorological stations, whereas the rate of loss corresponds to localized, event-based infiltration, interception and evapotranspiration. Until the mean precipitation exceeds the rate of loss, no overland flow occurs (Eq. 3).

$$pe_t = \begin{cases} p_t - f_c & \text{if } p_t > f_c \\ 0 & \text{otherwise} \end{cases} \quad \text{Eq. 3}$$

To transform the precipitation excess into overland flow, the kinematic wave method was applied in order to simulate the hydrologic flow in the river channel. This methodology is based on the continuity equation and a simplified form of the momentum equation. For the Cañete basin, we accounted for base flow in the river channel, and assessed the base flow from the sustained runoff during the dry period. The HEC-HMS model includes the constant monthly base flow model where the average discharge in the dry season is added to the overland flow computed for each time step of the simulation (Arlen, 2000).

3.2. Sediment transport model

The HEC-RAS model is capable of modelling sediment transport, comprising bed and suspended river load. Based on field observations, we assumed that the Cañete River is a transport-limited fluvial system in its middle and lower reach. We used the transport equation of Ackers and White (1973) in the HEC-RAS platform. It considers parameters of transport,

mobility and particle size, and is capable of distinguishing between fine and transitional particles (0.06 – 2mm), and coarse sediments (> 2mm). Equation 4 presents the non-dimensional transport function G_{gr} :

$$G_{gr} = C[(F_{gr} - A)/A]^m \quad \text{Eq. 4}$$

which depends on the sediment mobility non-dimensional parameter F_{gr} (Eq. 5):

$$F_{gr} = \frac{v_*^n}{\sqrt{gD(S-1)}} \left[\frac{V}{\sqrt{32 \log(10h/D)}} \right]^{1-n} \quad \text{Eq. 5}$$

where, v_* is the shear velocity (m/s), g the gravitational acceleration (m/s^2), D is the diameter of bed sediment (mm), S the specific gravity of sediments (non-dimensional), V the mean flow velocity (m/s), h is the effective flow depth (m), C and m are the coefficient and the exponent of transport formula respectively, A is the non-dimensional threshold of mobility, and n is a non-dimensional transition parameter.

Parameters n , m , A and C depend on the non-dimensional sediment size D_{gr} , described by Eq.

6. This parameter is capable of characterizing both suspended (fine and transitional sediments) and coarse sediments:

$$D_{gr} = D \left[\frac{g(S-1)}{v^2} \right]^{1/3} \quad \text{Eq. 6}$$

in which ν is the kinematic viscosity (m^2/s), and parameters D , g and S were described above.

For suspended sediment ($1 < D_{gr} < 60$) the parameters were calculated as follows (Eq. 7 to 10):

$$n = 1 - 0.56 \log D_{gr} \quad \text{Eq. 7}$$

$$A = 0.14 + \frac{0.23}{\sqrt{D_{gr}}} \quad \text{Eq. 8}$$

$$m = 1.67 + \frac{6.83}{D_{gr}} \quad \text{Eq. 9}$$

$$\log C = -3.46 + 2.79 \log D_{gr} \quad \text{Eq. 10}$$

For coarse sediment ($D_{gr} > 60$) we assumed the following values:

$$n = 0$$

$$A = 0.17$$

$$m = 1.78$$

$$C = 0.025$$

Thus, the sediment transport flux X (non-dimensional) is expressed as a solid mass flux per fluid mass flux (Eq. 11). The expression is based on G_{gr} (Eq. 4):

$$X = \frac{SD}{h} \left(\frac{V}{v_*} \right)^n G_{gr} \quad \text{Eq.11}$$

The parameters S , D , h , V , and v_* were described above.

To simulate bed sorting and armouring, HEC-RAS uses the Thomas mixing method (formerly Exner 5) that estimates the coarse armour or inactive layer which limits the transport capacity of a river (U.S. Army Corps of Engineering, 2016). The method describes the gradations of the active layer, which includes the cover and subsurface layers, in order to assess the transport capacity of the river.

Additionally, the particle fall velocity ω influences the ability to set a particle into motion, to keep it suspended, and to have it transported. The suspension of a particle is initiated once the bed-level shear velocity is similar to ω . Equation 12, proposed by Rubey (U.S. Army Corps of Engineering, 2016), is applicable to the entire range of particle sizes (e.g., gravel, sand, and

silt). The parameter F_1 equals 0.79 for particles $> 1 \text{ mm}$, and is derived using Eq. 13 for smaller particles.

$$\omega = F_1 \sqrt{(S-1)gD} \quad \text{Eq. 12}$$

$$F_1 = \sqrt{\frac{2}{3} + \frac{36v^2}{gD^3(S-1)}} - \sqrt{\frac{36v^2}{gD^3(S-1)}} \quad \text{Eq. 13}$$

The parameters included in Eq. 12 and 13 were already presented above.

3.3. Model calibration

To calibrate the hydrological and sediment transport model, the modelled discharge and sediment load were compared against stream flow and sediment measurements in the river channel. To assess the models' performance, five efficiency indexes were selected (Table 1), namely: The Nash-Sutcliffe efficiency (E), the coefficient of determination (r^2); the index of agreement (d); the relative volume bias (RVB); and the Kling-Gupta Efficiency (KGE). The first three are widely used in hydrological modelling (Krause et al., 2005). While the efficiency E is capable of evaluating basin dynamics, the disadvantage is that it presents the differences between the observed and predicted values as squared values. Thus, the highest values are overestimated, while the lowest ones are underestimated. The coefficient r^2 describes the combined dispersion against the single dispersion of the observed and predicted series. A value of 1 means that the dispersion of the prediction is equal to that of the observation. Unlike E , this parameter is not sensitive to over- or underestimated model outputs. The index d represents the ratio of the mean square error and the potential error where the numerator in the equation (Table 1) is sensitive to peak values, thereby overcoming the weakness of E and r^2 indexes. To account for low values, we also included the RVB index (Moussa and Chahinian, 2009). Finally, the KGE parameter (Gupta et al., 2009) is based on a multi-objective criterion that includes three components, namely: correlation, bias, and variability measures.

Table 1. Selected efficiency indexes to compare the observed (O_i) and projected (P_i) model outcomes. n is the total number of flood events used for calibration (Krause et al., 2005; Moussa and Chahinian, 2009).

Index	Equation	Value range	Optimal value
E	$E = 1 - \frac{\sum_{i=1}^n (O_i - P_i)^2}{\sum_{i=1}^n (O_i - \bar{O})^2}$	$< -\infty, 1 >$	1
r^2	$r^2 = \left(\frac{\sum_{i=1}^n (O_i - \bar{O})(P_i - \bar{P})}{\sqrt{\sum_{i=1}^n (O_i - \bar{O})^2} \sqrt{\sum_{i=1}^n (P_i - \bar{P})^2}} \right)^2$	$[0, 1]$	1
d	$d = 1 - \frac{\sum_{i=1}^n (O_i - P_i)^2}{\sum_{i=1}^n (P_i - \bar{O} + O_i - \bar{O})^2}$	$[0, 1]$	1
RVB	$RVB = \frac{\sum_{i=1}^n (P_i - O_i)}{\sum_{i=1}^n O_i}$	$[-1, +\infty >$	0
KGE	$KGE = 1 - \sqrt{(r - 1)^2 + (\beta - 1)^2 + (\gamma - 1)^2}$	$[0, 1]$	1

3.4. Data

3.4.1 Discharge and sediments

The hydrometeorology of the Cañete basin is monitored by a private company (Ambiand) that installed 12 meteorological ground stations (Fig. 5). Six of them record rainfall and temperature, five only rainfall and one only temperature. The meteorological data corresponds to daily precipitation (mm/day) and temperature (C°) collected over a 6-year period (2010 – 2015; Ambiand, unpublished data). We only used meteorological data recorded after the year 2010 as earlier records were discontinuous time-series (see Table 2). The basin contains 13 gauging stations, distributed along the river channel (Fig.5). These stations provided daily discharge data (m³/s), and we used the flow data from the years 2014-2015 (Ambiand, unpublished data) to calibrate the model. Six gauging stations that are situated

upstream of the Capillucas dam were selected for the hydrological model calibration, namely: Tanta, Azuchas, Huantan, Cacuciri, Putinza and Chavin gauging stations (Fig. 5).

Detailed information on sediment transport for Chavin gauging station is available from the private company CELEPSA (CELEPSA, unpublished data) that owns the El Platanal hydroelectric plant (Table 2). Before the construction of the Capillucas reservoir, sediment transport was measured several times a day during the months December to February (rainy season) of the four consecutive years 1998 to 2001. A total of 2465 water samples was collected at Chavin station using an US DH-48 depth-integrating suspended sediment sampler. Samples were analysed following the ASTM D3977 analysis method to determine the sediment concentration. At Chavin station, sediment concentrations of up to 12 g/l were measured. To obtain information on the spatial variation in sediment transport within the Cañete basin, a new monitoring campaign was organised from January 2018 to March 2018. During this campaign, water with suspended sediment samples were collected twice a day in 1 litre bottles using an US DH-48 depth-integrating suspended sediment sampler. A total of 256 sediment samples were collected at four stations: Chavin, Putinza, Huantan and Azuchas (Fig. 2, Fig. 5). The samples were analysed in the laboratory also following the Test Method B – Filtration from the ASTM Standard D3977 in order to determine sediment concentrations.

Table 2: Input data used to build the hydrological (HM) and sediment transport (STM) model.

Data	Source	Data period	Spatial resolution	Temporal resolution	Used as
Meteorological station (Rainfall and Temperature)	Ambiand	2010 - 2015	Point measurement	Daily	HM input
Gauging station	Ambiand	2014 - 2015	Point measurement	Daily	HM calibration
Suspended sediment samples	CELEPSA	1998 – 2001	Point measurement	Daily (rainfall season)	STM input
Suspended sediment samples		2018	Point measurement	Daily (rainfall season)	STM calibration
High resolution photographs		2018	Point measurement		STM input

3.4.2 Basin distribution and channel geometry

The Cañete river basin was divided into 25 sub-basins based on differences in altitude and climatological conditions (Fig. 2b). Fourteen lakes with surface areas larger than 0.4 km² (ANA, 2016) were modelled as natural reservoirs. Likewise, the Paucarcocha and Capillucas storage dams were included in the model domain. The model domain covered a length of about 228 km of the Cañete River. In the lower most reach the river enters a large extensional tectonic basin, and consequently the river channel widens significantly with less vertical incision. For this reach, we considered a trapezoidal channel shape, and estimated its dimensions from field observations and Google Earth images.

3.4.3 Bedload grain size

Image processing techniques were used to estimate the superficial grain size distribution of the bedload in the upper, middle-upper, middle and lower part reach of the Cañete River (e.g. Litty et al., 2017). A 1.5 m x 1.5 m square frame was placed on the gravel bars that were deposited on the proximal floodplain. It has been shown that by using a frame the bias induced through preferential sampling of the clasts is reduced (Bunte and Abt, 2001; Marcus et al., 1995). For each sample site, four high resolution photographs of the gravel bars were taken (Fig. 2b). The grain size distribution was calculated by digital image analysis techniques (Detert and Weitbrecht, 2012). The gravel bars of the upper reach contained mainly big boulders and some bedrock outcrops (Table 3), the ones of the middle and middle-upper reaches cobbles and pebbles (> 16mm) and sand particles; and the lower section contained small gravels and very fine particles (< 4 mm).

Table 3. Accumulative grain size distribution (%) for the upper, middle upper, middle and lower reach of the Cañete River.

Particle Diameter (mm)	Accumulative passing (% of particles smaller than...)			
	upper	middle upper	middle	lower
64	100.00	100.00	100.00	100.00
32	66.63	73.20	72.50	77.29
16	51.70	58.28	61.39	64.83
8	44.91	50.61	53.53	58.38
4	41.69	46.72	54.27	55.09

3.4.4 Rating curves

The gauging records (Table 2) were used to construct a rating curve to characterize the relationship between the water flow (Q) and the sediment load (Q_s). For the sediment data from CELEPSA at Chavin station, the curve was based on the average of the top 25% values to account for the maximum values. Since the 1998-2001 monitoring campaign took place before the construction of the Capillucas dam in 2006, the rating curve of 1998-2001 for Chavin station was assigned to the Putinza station located upstream of the dam (Fig. 5). Fig. 6 illustrates the power relation (with exponent = 2.5) between the sediment load and the discharge in the middle reach of the Cañete River. Here, the river transports water with low sediment concentrations (Fig. 6) during the dry season (i.e. 0.78 g/l for discharge of 50 m³/s), and high sediment concentration during discharge peaks (i.e. 3.08 g/l for 250 m³/s). The values are congruent with an earlier report from Morera et al. (2013).

Likewise, based on the data from our sediment monitoring campaign at Chavin, Putinza, Huantan and Azuchas stations in 2018 (Table 2), we derived sediment ratings curves for the four stations and assigned them to Chavin, Putinza, Huantan and Azuchas calibration sites (Fig. 7).

3.5. Scenarios of climate variability

A total of 10 climate change scenarios were constructed: a combination of two different precipitation patterns and five different precipitation amounts. The precipitation patterns (A and B) differ in the distribution of the rainfall change over the rainy season. Scenario A simulated the daily rainfall change distributed over the whole rainy season, while Scenario B distributed the variability over the moments with the highest precipitation only (i.e. the upper 99% percentile in the precipitation record). For each precipitation pattern (A and B), the amount of precipitation change was based on RCP2.6 and RCP8.5 climate change model simulations (Moss et al., 2008) from two Global Circulation models (GISS-E-H-p3 and MPI-ESM-MR). Table 4 gives an overview of the predicted change in seasonal rainfall by the GISS-E-H-p3 and MPI-ESM-MR models (Fluixa et al., 2018): for the 21st century, the change in precipitation ranges from -24% to +15% for the rainy season (December to February) and from -33% to +24% in the dry season (June to August). Based on Table 4, we generated 5 scenarios that included a variation of +5%, +8%, +10%, +15% and -17% of the total rainfall amount in the rainy season (Table 5).

Table 4. Seasonal rainfall changes of two Global Circulation models (GCM) from the Coupled Model Intercomparison Project Phase 5 (CMIP5). Emission scenarios: RCP 2.6 (optimist, high mitigation of gas emissions) and RCP 8.5 (pessimist, highest greenhouse gas emissions). After Fluixá et al. (2018).

GCM model	RCP scenarios	Future period	Rainfall season	Dry season
GISS-E-H-p3	RCP 2.6	2051 – 2075	- 14 %	+ 6 %
	RCP 2.6	2076 – 2100	- 17 %	+ 9 %
	RCP 8.5	2051 – 2075	- 24 %	+ 24 %
	RCP 8.5	2076 – 2100	- 14 %	+ 23 %
MPI-ESM-MR	RCP 2.6	2051 – 2075	+ 3 %	+ 9 %
	RCP 2.6	2076 – 2100	+ 6 %	- 4 %
	RCP 8.5	2051 – 2075	+ 9 %	- 33 %
	RCP 8.5	2076 – 2100	+ 15 %	- 1 %

Table 5: Projected rainfall scenarios for the Cañete basin. The change in precipitation rate has been applied to the rainy season (Dec. - Feb.).

Scenario group	Rainfall variation	Description
Scenario A	A + 5%	Precipitation change distributed over the whole rainy season
	A + 8%	
	A + 10%	
	A + 15%	
	A - 17%	
Scenario B	B + 5%	Precipitation change only over the periods of maximum rainfall
	B + 8%	
	B + 10%	
	B + 15%	
	B - 17%	

4. Results

4.1. Hydrological model

The results for six gauging stations present a marked increase in discharge including high flow rates during the rainy season (Dec. – Apr.) followed by a sustained low rate in the dry season (May. – Nov.) (Fig. 8). During most of the model runs the modelled data followed the same discharge pattern as the observed flow data. Likewise, the high r^2 and d values ($r^2 > 0.67$ and $d > 0.85$), and RVB of around zero in most of the stations (Table 6) are indicative for an acceptable model performance at the seasonal timescale (Bárdossy and Das, 2008; Singh and Bárdossy, 2012; Halwatura and Najim, 2013; Haberlandt and Radtke, 2014). Nevertheless, a constant underestimation of ~15 to 25% in the modelled discharge peaks was observed for the Tanta, Huantan, and Cacuciri stations (Fig. 8), while the model efficiency improved for the second half of the rainy season. The calibration indexes correspond to an acceptable hydrological model performance (Table 6), especially when considering the poor spatial distribution of the available hydro-meteorological data, and the heterogeneity in climate, topography, soils and vegetation.

Table 6: Calibration indexes obtained at the calibration sites for the hydrologic model. E : Nash-Nash-Sutcliff, r^2 : Coefficient of determination, d : index of agreement, RVB Relative volume bias and KGE : Kling-Gupta efficiency.

Hydrological model					
Control point	E	r^2	d	RVB	KGE
Tanta	0.590	0.692	0.861	- 0.319	0.632
Azuchas	0.651	0.670	0.897	- 0.059	0.819
Huantan	0.647	0.678	0.896	+ 0.045	0.734
Cacuciri	0.787	0.754	0.940	+ 0.071	0.663
Putinza	0.792	0.794	0.938	+ 0.040	0.807

Chavin	0.960	0.982	0.991	+ 0.100	0.897
--------	-------	-------	-------	---------	-------

4.2. Sediment transport model

Given that few data are available on sediment transport in the basin, the sediment transport model was calibrated here with the sediment loads that were derived from the 2018 rating curves (Q vs. Q_s) of the Chavin, Huantan, Azucha, and Putinza station (Fig. 7). The rating curves are based on the sediment concentration and discharge measurements in each control point (Fig.7). The model results are congruent with the overall spatial pattern of sediment loads within the Cañete catchment based on daily estimations. In general, the model results were acceptable with model efficiency indexes $r^2 > 0.5$, $d \sim 1$, and $E > 0.5$ for most stations, although the RVB and KGE indexes did not reach their optimum values (Table 7). A comparison between the rating curve-derived and modelled data showed that the highest modelled sediment loads (Q_s) were underestimated by 35% to 50% (Fig. 9). For Huantan station, the model underestimated sediment load by 80% at the end of the rainy season and the $r^2 (< 0.6)$ and $E (< 0.5)$ indexes showed low values even though the d parameter (> 0.7) reflected a good model performance. Similarly, the model underestimated in Azucha station the sediment load by about 0.5 kTon/day on average and 1 kTon/day during peak flows.

The sediment transport model predicts an annual sediment load of 981 kTon/yr at the Putinza calibration site, corresponding to a mean physical erosion rate of 0.12 mm/yr for the 3081 km² watershed upstream of Putinza station (Table 8). In the Capillucas storage dam, the model predicts a sediment accumulation of 217 kTon per year, corresponding to a siltation rate of 82 km³ per year. These values should be considered as minimum estimates, given the underestimation of the sediment loads by the sediment transport model (Table 7).

Table 7: Calibration indexes for the four calibration sites. E : Nash-Nash-Sutcliff, r^2 : Coefficient of determination, d : index of agreement, RVB Relative volume bias, KGE : Kling-Gupta Efficiency; ΔQ_s sediment load difference between modelled and observed data.

Sediment transport model						
Control point	E	r^2	d	RVB	KGE	ΔQ_s (10^3Ton/yr)
Azuchas	0.640	0.859	0.827	+ 0.228	0.333	13.949
Huantan	0.455	0.558	0.707	+ 0.309	0.221	58.992
Putinza	0.822	0.847	0.941	+ 0.093	0.679	64.279
Chavin	0.802	0.828	0.952	- 0.043	0.846	72.620

Table 8. Modelled sediment load at Putinza station and modelled amount of trapped sediments at Capillucas dam.

Drainage area (km ²)	Sample site elevation (m a.s.l.)	Sediment load		Physical erosion rate (mm/yr)	Trapped sediment	
		Ton/yr	m ³ /yr		Ton/yr	m ³ /yr
3 081	1 637	981 175	370 255	0.12	217 024	81 896

Sediment density: 2.65 Ton/m³

4.3. Scenario analyses

Figure 10 shows the rainfall runoff graphs for the middle part of the Cañete basin, based on the rainfall hyetograph for Yauyos meteorological station and the streamflow hydrograph for Putinza station. The graphs include the model run for 2014-2015, and the model outcomes for the eight projected rainfall scenarios with rainfall increases of +5%, +8%, +10% and +15%. As expected, an increase in precipitation rate led to an increase in streamflow. This increase is largest for the rainfall scenarios where the rainfall increase was distributed over the upper 99% percentile of the precipitation records.

A nonlinear relation was observed between the increment in the rainfall amount and the streamflow, with an abrupt increase in discharge when augmenting the rainfall amount with only +5%. Figure 11 illustrates the nonlinear response of the streamflow to changes in the rainfall amount for Putinza station: when increasing the rainfall amount with only +5%, the

average streamflow increased by 12 m³/s or 2 m³/s per % of rainfall increase. The increase in streamflow levels off to 0.4 and 0.5 m³/s per % of rainfall increase, when increasing the rainfall amount by an additional 3% (i.e. between +5% and +8%). For an equal amount of precipitation increase, the B scenarios (where the rainfall was distributed amongst the upper 99% percentile of rainfall events) showed the largest increase in average streamflow (Fig. 11).

The sediment load transported by the Cañete River was estimated at Putinza station. A positive relation exists between the rainfall increase and the sediment load in the river at Putinza (Fig. 12a), where an increase in rainfall amount leads to a nonlinear increase in sediment load. With an increase in rainfall amount between +5% and +10%, the sediment load increases only slightly with + 1.7% for the A scenario and increases proportionally with 5.5% for the B scenario. An additional increase in rainfall amount from +10% to +15% leads to a higher increase of 11.3% and 20% in sediment load per % of rainfall increase for the A and B scenarios, with maximum sediment loads of 1.1 MTon/yr (scenario A+15%) and 1.3 MTon/yr (scenario B+15%). Besides the nonlinear response of sediment load to precipitation increments, the model simulations showed that the rainfall pattern plays an important role in controlling sediment transport: in all cases, the B scenarios led to higher sediment loads than the A scenarios (Fig. 12a). For example, an increase in discharge with +15% resulted in sediment loads that were 195 kTon/yr higher for the B compared to the A scenario.

The change in sediment load in the river channel has consequences for the siltation rate in the storage reservoir of Capillucas. The sediment that is delivered to the dam progressively reduced the water storage capacity of the reservoir (Fig. 12c). Using the 2014-2015 calibration dataset, the average life cycle of the Capillucas dam is estimated at 17 years. Our results suggested that a regular increase in the precipitation of +5% and +15% might reduce the useful life to resp. 16 and 10 years. When the increase in precipitation occurred during the peak

rainfall events only, then the life cycle of the reservoir is rapidly reduced to respectively 13 and 7 years for scenario B +5% and B+15%. Scenarios A-17% and B-17% were the most optimistic scenarios, with a reduction of ~900 Ton/yr in the sediment load and trapped sediment volume, and subsequent increase in the life cycle of the reservoir to 27 (A -17%), and 31 years (B -17%) (Fig.12a and 12b).

5. Discussion

5.1. Limitations of gauge-based sediment load measurements

One of the main issues to assess the impact climate change will have on fluvial systems is the scarcity of observed hydrometeorological data (Guyot, 2007; Lavado, 2012; Rau, 2017).

Commonly, the spatial distribution of rainfall and discharge measurement stations is limited and the recorded data do not present continuous time series. This is especially true for the Andean countries (Latubresse and Restrepo, 2015). Our hydrological model yielded average calibration indexes for most of the gauging stations (Fig.8), but underestimated discharge peaks. This is probably related to the temporal resolution of the input data. The daily resolution of the data allowed us to simulate the overall pattern of daily discharge, but to have an adequate representation of peak discharges, the input data need to have a finer (i.e. hourly) resolution (Beven, 2012). The underestimation of the modelled sediment transport for some of the stations is likely because of the limited sediment concentration data used to build the sediment rating curves (Fig. 6 y 7). This will likely have a significant impact on our modelling outcomes as the Cañete River is a transport-limited system. The limitations of rating curves to represent the large variations in sediment load related to seasonal effects and antecedent conditions in river basin were identified in a large range of climate conditions (Walling, 1977; Asselman, 2000; Moges et al., 2016; Tenorio et al., 2018). Likewise, the short duration of the sediment monitoring campaigns for both the modelling (only one sampling station) and the

calibration (only one campaign during the 2018 rainy season) exercises limit model performance. Even so, other issues like change in grain size distribution or error propagation from the hydrological model outcomes might also play a role.

Furthermore, estimating sediment yields bases on stream-gauge measurements strongly depends on (i) the assumption of stationarity in the flood records; and (ii) the reliability of the sediment rating curves for extreme discharge events. It is likely that climate variability due to the influence of ENSO in the Cañete basin will affect the assumption of an evenly distributed frequency of flood events (Machado et al., 2015; Molina et al., 2015). In addition, the sediment rating curve (Fig. 6) that was used as input of the sediment transport model was based on observations of total suspended solids.

Although the range of flow rates during the 1998-2001 monitoring period is not different from the daily flow rates of the model simulations, it is clear from Figs. 6 and 7 that the sediment concentration data is heteroskedastic. The sediment load estimates derived from the limited gauge data are therefore associated with larger uncertainty for high and very high flow rates. Fig. 6 illustrates how the sediment rating curve at Chavin station (before the construction of the dam) fails to predict the > 3 g/l sediment concentrations observed at very high flow rates of > 250 m³/s (Fig. 6). This affects the precision of the sediment transport model, where the annual sediment load is reasonably well predicted notwithstanding the underestimation of the sediment load during extreme events.

5.2. Potential impact of climate variability on water storage capacity of hydroelectric reservoirs

The coupled hydrological-sediment transport model calibrated for the 2014-2015 period predicted a sediment load of 981 kTon/yr or 370 km³/yr or 318 Ton/ km² yr upstream of the Capillucas reservoir. Our estimates for the Cañete River are lower than the sediment fluxes that were reported by Morera et al. (2013) and Latrubesse and Restrepo (2014) for the

northern Peruvian coast, where modern sediment fluxes of 779 and 1,000 Ton/ km² yr were reported. The latter rivers are located along the northern coast where ENSO events periodically trigger high rainfall rates and a significant increase in river discharge. The modern physical erosion rate of 0.12 mm/yr (or 981 kTon/yr) for Putinza station (Table 8) is in line with published ¹⁰Be-derived denudation rates of the Cañete and adjacent river systems. The ¹⁰Be-derived denudation rates integrate over 10³ to 10⁴ years, and are representative for the long-term denudation rates of the basin (Vanacker et al., 2015). Reber et al. (2017) reported ¹⁰Be-derived denudation rates of 0.05 mm/yr for the lower reach of the Cañete River, where the river is located in a wide alluvial valley flanked by low gradient hillslopes. In adjacent catchments south of Cañete, ¹⁰Be-derived catchment-wide denudation rates of 0.08 to 0.13 mm/yr were reported by Abbühl et al. (2011) and Bekaddour et al. (2014).

Along the Peruvian Coastal Range, a strong relation between rainfall amount and sediment load is expected based on previous works (e.g. Morera et al., 2013). The interannual rainfall pattern plays an important role where ENSO events induce high rainfall rates over a short time as shown by the modelled B scenarios. Therefore, a very high amount of sediment production can be expected during such episodic events. This is corroborated by data from the Piura region in northern Peru, which is highly susceptible to ENSO events. Here, a sediment flux of 20 MTon/yr (Latrubesse and Restrepo, 2014) or a maximum denudation rate of 0.185 mm/yr (Abbühl et al., 2011) was calculated for ENSO events. The northern Peruvian Jequetepeque River basin exhibits high erosion rates of 0.1 to 0.9 mm/yr during ENSO events (Estrada et al., 2009; Pepin et al., 2013). A context similar to ENSO events is performed by scenarios B+10% and B+15% that investigated the occurrence of extreme precipitation, resulting in a denudation rate of 0.13 and 0.16 mm/yr respectively. However, most of the published denudation studies represent average values over geological time scales. There is a lack of quantitative analysis of contemporary erosion and denudation rates for extreme events such

as ENSO but observations from a recent (coastal) El Niño event in 2017 (INDECI, 2017) show that the denudation rates are likely 1-2 orders of magnitude higher than indicated in the aforementioned studies (Abbühl et al., 2011; Estrada et al., 2009; Pepin et al., 2013).

Furthermore, these recent events also provide insights into physical mechanisms of sediment transport dynamics. Especially in the dry, middle and lower reaches of the Cañete River, ephemeral tributary channels are activated during extreme rainfall events and transport large sediment loads to the Cañete River where virtually all gauging stations are located. The tributaries are typically discharge-limited and not sediment limited. So, due to its climatic and geologic conditions sediment production and transport dynamics in the Cañete catchment are strongly driven by extreme events which makes the modelling of transport dynamics challenging.

Our results furthermore suggested an average sedimentation rate into the Capillucas reservoir of 217 kTon/yr or 82 km³/yr or 1.3 MTon/yr per km² of reservoir surface (Table 8). Under extreme ENSO-induced conditions the calculated rates were 2.1MTon/yr and 3.4 MTon/yr per km² of reservoir surface (Fig. 12b) for scenarios B+10% and B+15% respectively. Likewise, our model results suggested a strong relationship between the stored sediment, the rainfall amount and rainfall pattern. It is worth stressing the fact that the impact of exogenous geomorphic hazards (e.g. dam sedimentation) has devastating consequences in developing countries (Alcantara-Ayala, 2002). Despite its limitations, the methodology we propose is highly replicable and could be used to assess other dams in developing countries. Most studies related to sediment transport in Peru were focused so far at the principal national reservoirs that are periodically impacted by ENSO. The Gallito Ciego reservoir trapped 5.1 Mm³/yr (1 MTon/yr per km² of reservoir surface) between the years 1991 to 2007 (Walter et al., 2012). Equally, the Poechos reservoir trapped a maximum sediment flux of 113 MTon/yr (2 MTon/yr per km² of superficial area (Tote et al., 2011). Those rates are very similar to the ones observed

in the Cañete basin and show that the Peruvian hydroelectric reservoirs are very vulnerable to climate variability. With an annual increase of 8% in energy demand and strong impulse of the hydroelectric sector, Peru is in a prime position to push for sustainable development of the hydroelectric sector.

Journal Pre-proofs

6. Conclusions

The amount of sediment transported in Andean rivers may increase over the next years due to climate variability and change. As a result, hydroelectric reservoirs could be silting up more rapidly than anticipated. The methodology presented in this paper coupled a hydrological and sediment transport model to model the sediment load of the 6,049-km²-large Cañete River basin in the Peruvian Andes. Ten climate change scenarios were developed to evaluate the potential impact of precipitation change on stream discharge and sediment load. The model outcomes showed that the amount of precipitation as well as the precipitation pattern controls the amount of sediment transported by the Cañete River. The sediment load presents a nonlinear, positive exponential relationship with the change in precipitation rate, thereby showing the importance of extreme climate events on sediment load. A simulation of transported sediments influenced by a 15%-increase in the moments of highest precipitation shows that peak discharge Q_p may increase with 34%. The average sediment load was estimated at 981 175 Ton/yr, or 0.12 mm/yr upstream of the Capillucas reservoir, which is in agreement with published denudation rates for the area. Our results show that the lifespan of the Capillucas reservoir ranges from 7 years for the most pessimistic scenario to 31 years for the most optimistic scenario. This is much shorter than the projected lifespan of 50 years. Peru currently has a large growth in energy demand of 8% per year and has pushed a significant growth in hydroelectricity of all Andean countries. But Peru is also expected to be strongly affected by climate change. Our pilot study therefore shows that silting of hydroelectric reservoirs may become a serious issue if counter measures are not taken.

Acknowledgements

This study was supported by the Proyecto Glaciares+, implemented by CARE Peru and the University of Zurich and funded by the Swiss Agency for Development and Cooperation (SDC), and by the ARES POP project on “Erosion and sediment yield in response to climate change and variability” funded by the Coopération au développement de l’Académie de Recherche et d’Enseignement supérieur. Miluska Rosas was supported by a PhD Scholarship from the Conseil de l’Action Internationale from UCLouvain (Grant No. ADRI/CD/CA/2016-NR 51).

Journal Pre-proofs

References

- Aalto, R., Dunne, T., and Guyot, J. L. (2006). Geomorphic Controls on Andean Denudation Rates. *The Journal of Geology*, 114(1), 85–99. <https://doi.org/10.1086/498101>
- Abbühl, L. M., Norton, K. P., Jansen, J. D., Schlunegger, F., Aldahan, A., and Possnert, G. (2011). Erosion rates and mechanisms of knickzone retreat inferred from ¹⁰Be measured across strong climate gradients on the northern and central Andes Western Escarpment. *Earth Surface Processes and Landforms*, 36(11), 1464–1473. <https://doi.org/10.1002/esp.2164>
- Alcántara-Ayala, I. (2002). Geomorphology, natural hazards, vulnerability and prevention of natural disasters in developing countries. *Geomorphology*, 47(2-4), 107-124. [https://doi.org/10.1016/S0169-555X\(02\)00083-1](https://doi.org/10.1016/S0169-555X(02)00083-1)
- Amini, A., Heller, P., De Cesare, G., Schleiss, A., Schleiss, A., Franca, M. J., and Pfister, M. (2014). Comprehensive numerical simulations of sediment transport and flushing of a Peruvian reservoir. *Proceedings of River Flow 2014, Special Session on Reservoir Sedimentation*, 211-219. Lausanne, Switzerland.
- ANA. (2010). Recursos hídricos del Perú en cifras, Reporte Técnico. Oficina del Sistema Nacional de Información de Recursos Hídricos de la Autoridad Nacional del Agua - OSNIRH ANA. Lima.
- ANA. (2016). *Inventario nacional de glaciares y lagunas*. Ediciones ANA. Lima.
- ANA. (2017). *Compendio Nacional de Estadísticas de Recursos Hídricos 2016*. Lima.
- Annandale, G.W., Morris, G. L., and Karki, P. (2016). Extending the Life of Reservoirs, Sustainable Sediment Management for Dams and Run-of-River Hydropower. World Bank Group. Washington DC, USA.
- Aouad, G., Laboudigue, A., Gineys, N., and Abriak, N. E. (2012). Dredged sediments used as novel supply of raw material to produce Portland cement clinker. *Cement and Concrete Composites*, 34(6), 788–793. <https://doi.org/10.1016/j.cemconcomp.2012.02.008>
- Arlen D, F. (2000). Hydrologic Modeling System HEC-HMS Technical Reference Manual. US

- Army Corps of Engineers*, (March), 155. <https://doi.org/CDP-74B>
- Asselman, N.E.M. (2000). Fitting and interpretation of sediment rating curves. *Journal of Hydrology*, 234(3-4), 228-248. [https://doi.org/10.1016/S0022-1694\(00\)00253-5](https://doi.org/10.1016/S0022-1694(00)00253-5)
- Aybar Camacho, C., and Lavado-Casimiro, W. (2017). *Mapa de Zonas de Vida del Perú*. Lima. Retrieved from <http://idesepe.senamhi.gob.pe/geonetwork/srv/spa/catalog.search;jsessionid=478A7A984D6898BF8C2D8F8E553F1AB2#/metadata/8266683e-dc79-413e-bbd2-aca640b1f1e8>
- Bárdossy, A., and Das, T. (2008). Influence of rainfall observation network on model calibration and application. *Hydrology and Earth System Sciences Discussions*, 12 (1), 77–89.
- Bekaddour, T., Schlunegger, F., Vogel, H., Delunel, R., Norton, K. P., Akçar, N., and Kubik, P. (2014). Paleo erosion rates and climate shifts recorded by Quaternary cut-and-fill sequences in the Pisco valley, central Peru. *Earth and Planetary Science Letters*, 390, 103–115. <https://doi.org/10.1016/j.epsl.2013.12.048>
- Beven, K. (2012). *Rainfall-Runoff Modelling The Primer SECOND EDITION*. Retrieved from www.wiley.com/wiley-blackwell.
- Bunte, K., and Abt, S. (2001). Summary for Policymakers. *Climate Change 2013 - The Physical Science Basis*, 1–30. <https://doi.org/10.1017/CBO9781107415324.004>
- Cadilhac, L., Torres, R., Calles, J., Vanacker, V., and Calderón, E. (2017). Desafíos para la investigación sobre el cambio climático en Ecuador. *Neotropical Biodiversity*, 3:1, 168-181. <https://doi.org/10.1080/23766808.2017.1328247>
- Chang, C. L., Lo, S. L., and Yu, S. L. (2005). Interpolating precipitation and its relation to runoff and non-point source pollution. *Journal of Environmental Science and Health - Part A Toxic/Hazardous Substances and Environmental Engineering*, 40(10), 1963–1973. <https://doi.org/10.1080/10934520500184673>
- Chou, S. C., Lyra, A., Mourão, C., Dereczynski, C., Pilotto, I., Gomes, J., ... Marengo, J. (2014). Assessment of Climate Change over South America under RCP 4.5 and 8.5 Downscaling

Scenarios. *American Journal of Climate Change*, 03(05), 512–527.

<https://doi.org/10.4236/ajcc.2014.35043>

Clark, K.E., West, A.J., Hilton, R.G., Asner, G.P., Quesada, C.A., Silman, M.R., Saatchi, S.S.,

Farfan-Rios, W., Martin, R.E., Horwath, A.B., Halladay, K., New, M., Malhi, Y. (2016).

Storm-triggered landslides in the Peruvian Andes and implications for topography, carbon cycles, and biodiversity; *Earth Surface Dynamics*, 4 (1), 47-70.

<https://doi.org/10.5194/esurf-4-47-2016>

Coustau, M., Bouvier, C., Borrell-Estupina, V., & Jourde, H. (2012). Flood modelling with a

distributed event-based parsimonious rainfall-runoff model: case of the karstic Lez river catchment. *Natural Hazards and Earth System Sciences*, 12(4), 1119-1133.

<https://doi.org/10.5194/nhess-12-1119-2012>

Detert, M., and Weitbrecht, V. (2012). Automatic object detection to analyze the geometry of

gravel grains—a free stand-alone tool. *River Flow 2012*, (August 2016), 595–600. Retrieved from

http://people.ee.ethz.ch/~vawweb/publications/river_engineering_division_vaw/2012_3125.pdf

Diouf, O. C., Weihermüller, L., Ba, K., Faye, S. C., Faye, S., and Vereecken, H. (2016). Estimation

of Turc reference evapotranspiration with limited data against the Penman-Monteith

Formula in Senegal. *Journal of Agriculture and Environment for International*

Development -JAEID, 110(1), 117–137. <https://doi.org/10.12895/jaeid.20161.417>

Estrada, R. D., Quintero, M., Moreno, A., and Ravnborg, H. M. (2009). *Payment for*

Environmental Services as a Mechanism for Promoting Rural Development in the Upper

Watersheds of the Tropics. Retrieved from

https://assets.publishing.service.gov.uk/media/57a08b6be5274a27b2000b1d/PN22_CO NDESAN_ProjectReport_Oct09_final.pdf

Fluixá, J., García Hernández, J., Huggel, C., Frey, H., Muñoz, R., Barriga, L., ... Nuñez, J. (2018).

- Resumen Ejecutivo: Modelización hidrológica de la cuenca del Cañete y evaluación del impacto del cambio climático en los recursos hídricos, Proyecto Glaciares, Lima, Peru.
- Gupta, H. V., Kling, H., Yilmaz, K. K., and Martinez, G. F. (2009). Decomposition of the mean squared error and NSE performance criteria: Implications for improving hydrological modelling. *Journal of Hydrology*, 377(1–2), 80–91.
<https://doi.org/10.1016/j.jhydrol.2009.08.003>
- Guyot J.L., Bazan, H., Fraizy, P., Ordoñez, J.J., Armijos, E. and Laraque, A. (2017). Suspended sediment yields in the Amazon basin of Peru: a first estimation. *Water Quality and Sediment Behaviour of the Future: Predictions for the 21st Century*. Proceedings of Symposium HS2005 at IUGG2007, Perugia, July 2007.
- Haberlandt, U., and Radtke, I. (2014). Hydrological model calibration for derived flood frequency analysis using stochastic rainfall and probability distributions of peak flows. *Hydrology and Earth System Sciences*, 18, 353-365. [http:// doi:10.5194/hess-18-353-2014](http://doi:10.5194/hess-18-353-2014)
- Halwatura, D. and Najim, M. M. M. (2013). Application of the HEC-HMS model for runoff simulation in a tropical catchment. *Environmental Modelling & Software*, 46, 155-162.
<https://doi.org/10.1016/j.envsoft.2013.03.006>.
- Hauer, C., Wagner, B., Aigner, J., Holzapfel, P., Flödl, P., Liedermann, M., ... Habersack, H. (2018). State of the art, shortcomings and future challenges for a sustainable sediment management in hydropower: A review. *Renewable and Sustainable Energy Reviews*, 98(January), 40–55. <https://doi.org/10.1016/j.rser.2018.08.031>
- Instituto Nacional de Defensa Civil - INDECI. (2012). *INFORME DE EMERGENCIA N° 335 Precipitaciones pluviales que afecta distritos de Lima - Provincias*. Lima. Retrieved from www.indeci.gob.pe
- Instituto Nacional de Defensa Civil - INDECI. (2017). *INFORME DE EMERGENCIA N° 264 Precipitaciones pluviales en la provincia de Cañete - Lima*. Lima.
- INEI. (2017). *Compendio Estadístico Lima Provincias 2016*. Lima. Retrieved from

www.inei.gob.pe

- Krause, P., Boyle, D. P., and Bäse, F. (2005). Comparison of different efficiency criteria for hydrological model assessment. *Advances in Geosciences*, 5, 89–97.
<https://doi.org/10.5194/adgeo-5-89-2005>
- Latrubesse, E. M., and Restrepo, J. D. (2014). Sediment yield along the Andes: Continental budget, regional variations, and comparisons with other basins from orogenic mountain belts. *Geomorphology*, 216, 225–233. <https://doi.org/10.1016/j.geomorph.2014.04.007>
- Latrubesse, E. M., Stevaux, J. C., and Sinha, R. (2005). Tropical rivers. *Geomorphology*, 70, 187–206. <https://doi.org/10.1016/j.geomorph.2005.02.005>
- Lavado, W., Ronchail, J., Labat, D., Espinoza, J.C., and Guyot, J.L. (2012). Basin-scale analysis of rainfall and runoff in Peru (1969–2004): Pacific, Titicaca and Amazonas drainages, *Hydrological Sciences Journal*, <https://doi.org/10.1080/02626667.2012.672985>
- Litty, C., Schlunegger, F., and Viveen, W. (2017). Possible threshold controls on sediment grain properties of Peruvian coastal river basins. *Earth Surface Dynamics*, 5(3), 571–583.
<https://doi.org/10.5194/esurf-5-571-2017>
- Marcus, W. A., Ladd, S. C., Stoughton, J. A., and Stock, J. W. (1995). Pebble Counts and The Role of User-Dependent Bias in Documenting Sediment Size Distributions. *Water Resources Research*, 31(10), 2625–2631. <https://doi.org/10.1029/95WR02171>
- Marengo, J. A., Ambrizzi, T., da Rocha, R. P., Alves, L. M., Cuadra, S. V., Valverde, M. C., ... Ferraz, S. E. T. (2010). Future change of climate in South America in the late twenty-first century: Intercomparison of scenarios from three regional climate models. *Climate Dynamics*, 35(6), 1089–1113. <https://doi.org/10.1007/s00382-009-0721-6>
- McCuen, R. H. (1998). *Hydrologic analysis and design*. Upper Saddle River, N.J: Prentice Hall.
- Moges, M.A., Zemale, F.A., Alemu, M.L., Ayele, G.K., Dagnew, D.C., Tilahun, S.A. and Steenhuis, T.S. (2016). Sediment concentration rating curves for a monsoonal climate: upper Blue Nile. *Soil*, 2(3), 337-349. <https://doi:10.5194/soil-2-337-2016>

- Molina, A., Vanacker, V., Brisson, E., Mora, D., Balthazar, V. (2015). Multidecadal change in streamflow associated with anthropogenic disturbances in the tropical Andes. *Hydrology and Earth System Sciences*, 19 (10), pp. 4201-4213. <https://doi.org/10.5194/hess-19-4201-2015>
- Molina, A., Govers, G., Poesen, J., Van Hemelryck, H., De Bièvre, B., Vanacker, V. (2008). Environmental factors controlling spatial variation in sediment yield in a central Andean mountain area, *Geomorphology*, 98 (3–4), 176-186. <https://doi.org/10.1016/j.geomorph.2006.12.025>.
- Morera, S. B., Condom, T., Vauchel, P., Guyot, J. L., Galvez, C., and Crave, A. (2013). Pertinent spatio-temporal scale of observation to understand suspended sediment yield control factors in the Andean region: The case of the Santa River (Peru). *Hydrology and Earth System Sciences*, 17(11), 4641–4657. <https://doi.org/10.5194/hess-17-4641-2013>
- Morris, G. L., Annandale, G. W., and Hotchkiss, R. (2008). Reservoir Sedimentation. In *Sedimentation Engineering Processes Measurements Modeling and Practice ASCE Manuals and Reports on Engineering Practice No 110*. <https://doi.org/10.2134/jeq2006.0296>
- Moss, R., Babiker, M., Brinkman, S., Calvo, E., Carter, T., Edmonds, J., Elgizouli, I., Emori, S., Erda, L., Hibbard, K., Jones, R., Kainuma, M., Kelleher, J., Lamarque, J. F., Manning, M., Matthews, B., Meehl, J., Meyer, L., Mitchell, J., Nakicenovic, N., O'Neill, B., Pichs, R., Riahi, R., Rose, S., Runci, P., Stouffer, R., van Vuuren, D., Weyant, J., Wilbanks, T., van Ypersele, J. P., and Zurek, M. (2008). *Towards New Scenarios for Analysis of Emissions, Climate Change, Impacts, and Response Strategies*. Technical Summary. Intergovernmental Panel on Climate Change, Geneva, 25 pp.
- Moussa, R., and Chahinian, N. (2009). Comparison of different multi-objective calibration criteria using a conceptual rainfall-runoff model of flood events. *Hydrology and Earth System Sciences*, 13(4), 519–535. <https://doi.org/10.5194/hess-13-519-2009>

- Naipal, V., Reick, C., Pongratz, J., and Van Oost, K. (2015). Improving the global applicability of the RUSLE model - Adjustment of the topographical and rainfall erosivity factors. *Geoscientific Model Development*, 8(9), 2893–2913. <https://doi.org/10.5194/gmd-8-2893-2015>
- Navarro Colque, P. A. (2016). *Mapa Geológico del Perú 1:1 000 000*. Retrieved from <http://www.ingemmet.gob.pe/mapa-geologico-nacional>
- Nicholson, S. E. (2011). *Dryland climatology*. *Dryland Climatology*. <https://doi.org/10.1017/CBO9780511973840>
- Ochoa, M., Moreno, J., Rodriguez, R., Fabián, C., Nuñez, S., and Gómez, D. (2017). *Evaluación Geológica de las zonas afectadas por el Niño Costero 2017 en las regiones Lima-Ica*. Lima. Retrieved from http://sigrid.cenepred.gob.pe/docs/PARA PUBLICAR/INGEMMET/Informe_Tecnico_A_6768_Geologica_de_las_zonas_afectadas_por_el_nino_costero_Lima_Ica_2017.pdf
- Palmieri, A., Shah, F., Annandale, G. W., and Dinar, A. (2003). *Reservoir Conservation Volume I: The RESCON Approach Economic and engineering evaluation of alternative strategies for managing sedimentation in storage reservoirs*. Retrieved from <http://documents.worldbank.org/curated/en/819541468138875126/pdf/349540v10Reservoir0conservation0RESCON.pdf>
- Pepin, E., Carretier, S., Guyot, J. L., and Escobar, F. (2010). Specific suspended sediment yields of the Andean rivers of Chile and their relationship to climate, slope and vegetation. *Hydrological Sciences Journal*, 55(7), 1190–1205. <https://doi.org/10.1080/02626667.2010.512868>
- Pepin, E., Guyot, J.L., Armijos, E., Bazán, H., Fraizy, P., Moquet, J.S., Noriega, L., Lavado, W., Pombosa, R. and Vauchel, P. (2013). Climatic control on eastern Andean denudation rates (Central Cordillera from Ecuador to Bolivia). *Journal of South American Earth Sciences*, 44, 85-93. <https://doi.org/10.1016/j.jsames.2012.12.010>

Pereira, J.F., McCorquodale, E.A., Meselhe, E.A., Georgiou, I.Y., and Allison, M.A. (2009).

Numerical Simulation of Bed Material Transport in the Lower Mississippi River. *Journal of Coastal Research*, SI 56 (Proceedings of the 10th International Coastal Symposium), 1449-1453. Lisbon, Portugal, ISSN 0749-0258.

Ramírez, C., and Cisneros, H. (2007). *Andean System of Basins: Watershed Profiles Enhancing Agricultural Water Productivity Through Strategic Research*. Lima. Retrieved from www.cipotato.org

Rau, P., Bourrel, L., Labat, D., Melo, P., Dewitte, B., Frappart, F., ... Felipe, O. (2017).

Regionalization of rainfall over the Peruvian Pacific slope and coast. *International Journal of Climatology*, 37(1), 143–158. <https://doi.org/10.1002/joc.4693>

Reber, R., Delunel, R., Schlunegger, F., Litty, C., Madella, A., Akçar, N., and Christl, M.

(2017). Environmental controls on 10Be-based catchment-averaged denudation rates along the western margin of the Peruvian Andes. *Terra Nova*. 29, 282–293. <https://doi.org/10.1111/ter.12274>

Restrepo, J. D., and Syvitski, J. P. M. (2006). Assessing the Effect of Natural Controls and Land Use Change on Sediment Yield in a Major Andean River: The Magdalena Drainage Basin, Colombia. *AMBIO: A Journal of the Human Environment*, 35(2), 65–74.

[https://doi.org/10.1579/0044-7447\(2006\)35\[65:ATEONC\]2.0.CO;2](https://doi.org/10.1579/0044-7447(2006)35[65:ATEONC]2.0.CO;2)

Roman-Gonzalez, A., Meneses-Claudio, B.A., Vargas-Cuentas, N.I. (2019). Flood analysis in Peru using satellite image: The Summer 2017 case. *International Journal of Advanced Computer Science and Applications*, 10 (2), 346-351.

<http://dx.doi.org/10.14569/IJACSA.2019.0100246>

Sistema Nacional para la prevención y atención de Desastres - SINPAD (2017). Estado

Situacional de la Emergencia, Emergencias: 00083655, 00083838, 00083840, 00083841, 00083861, 00083864, 00084015, 00084033, 00084279, 00084410 y 00084809. INDECI, Lima, Peru.

- Singh, S. K., and Bárdossy, A. (2012). Calibration of hydrological models on hydrologically unusual events. *Advance Water Resources*, 38, 81–91.
<http://doi:10.1016/j.advwatres.2011.12.006>, 2012.
- Sheehan, C., Harrington, J., and Murphy, J. D. (2010). A technical assessment of topsoil production from dredged material. *Resources, Conservation and Recycling*, 54(12), 1377–1385. <https://doi.org/10.1016/j.resconrec.2010.05.012>
- Sucozhañay, A., and Céleri, R. (2018). Impact of Rain Gauges distribution on the runoff simulation of a small mountain catchment in Southern Ecuador. *Water (Switzerland)*, 10(9). <https://doi.org/10.3390/w10091169>
- Sutherland, W. J., Bardsley, S., Clout, M., Depledge, M. H., Dicks, L. V., Fellman, L., Fleishman, E., Gibbons, D. W., Keim, B., Lickorish, F., Margerison, C., Monk, K. A., Norris, K., Peck, L. S., Prior, S. V., Scharlemann, J. P.W., Spalding, M. D., and Watkinson, A. R. (2013). A horizon scan of global conservation issues for 2013, *Trends in Ecology and Evolution*, 28(1), 16-22. <https://doi.org/10.1016/j.tree.2012.10.022>.
- Tamayo, J., Salvador, J., Vasquez, A., Vilches, C., Edici, P., and Alberto, C. (2016). *La industria de la electricidad en el Perú: 25 años de aportes al crecimiento económico del país*. Osinergmin. Lima. <https://doi.org/978-612-47350-0-4>
- Tenorio, G.E., Vanacker, V., Campforts, B., Álvarez, L., Zhiminaicela, S., Vercruyssen, K., Molina, A., and Govers, G. (2018). Tracking spatial variation in river load from Andean highlands to inter-Andean valleys. *Geomorphology*, 308, 175-189.
<https://doi.org/10.1016/j.geomorph.2018.02.009>
- Tote, C., Govers, G., Van Kerckhoven, S., Filiberto, I., Verstraeten, G., and Eerens, H. (2011). Effect of ENSO events on sediment production in a large coastal basin in northern Peru. *Earth Surface Processes and Landforms*, 36(13), 1776–1788.
<https://doi.org/10.1002/esp.2200>
- U.S. Army Corps of Engineering. (2016). HEC-RAS 5.0 Hydraulic Reference Manual, (February),

547. <https://doi.org/CPD-68>
- Vanacker, V., von Blanckenburg, F., Govers, G., Molina, A., Campforts, B., Kubik, P.W. (2015). Transient river response, captured by channel steepness and its concavity. *Geomorphology*, 228, 234–243. <https://doi.org/10.1016/j.geomorph.2014.09.013>.
- Viveen, W., and Schlunegger, F. (2018). Prolonged extension and subsidence of the Peruvian forearc during the Cenozoic. *Tectonophysics*, 730(February), 48–62. <https://doi.org/10.1016/j.tecto.2018.02.018>
- Vuille, M., Carey, M., Huggel, C., Buytaert, W., Rabatel, A., Jacobsen, D., Soruco, A., Villacis, M., Yarleque, C., Elison Timm, O., Condom, T., Salzmann, N., Sicart, J.-E. (2018). Rapid decline of snow and ice in the tropical Andes – Impacts, uncertainties and challenges ahead. *Earth-Science Reviews*, 176, pp. 195-213. <https://doi.org/10.1016/j.earscirev.2017.09.019>
- Walling, D.E. (1977). Limitations of the rating curve technique for estimating suspended sediment loads, with particular reference to British rivers. In *Erosion and solid matter transport in inland waters*. Vol. 122, 34-48. IAHS Publication.
- Walter, K., Gunkel, G., and Gamboa, N. (2012). An assessment of sediment reuse for sediment management of Gallito Ciego Reservoir, Peru. *Lakes and Reservoirs: Research and Management*, 17(4), 301–314. <https://doi.org/10.1111/lre.12008>
- WEC - Water Energy Council. (2010). *Water for Energy*. London. www.worldenergy.org ISBN: 978-0-946121-10-6.
- World Bank. (2017). International bank for reconstruction and development international finance corporation and multilateral investment guarantee agency country partnership framework for the republic of Peru for the period FY17-FY21. Report No. 112299-PE.

Captions

Figure 1.

Cañete river basin. Location of the basin within southern Peru, with indication of rural centres, and location of the Capillucas storage dam.

Figure 2.

Physiographic characteristics of the Cañete basin, (a) Lithology map (Navarro Colque, 2016) and (b) Sub-division of the basin in four zones: lower, middle, middle upper and upper sections of the basin (Aybar Camacho and Lavado-Casimiro, 2017).

Figure 3.

Flow diagram of the proposed methodology.

Figure 4.

Representation of basin precipitation-runoff process, adapted from (Arlen, 2000).

Figure 5.

Spatial distribution of meteorological ground stations (rainfall and temperature data) and flow measurement (gauging) stations in Cañete basin.

Figure 6.

Relation of suspended sediment concentration, SSC, and discharge (left side), and rating curve assigned (right side) to Putinza station. The data was collected at Chavin gauging station over the periods 1998-99, 2000 and 2001 before the construction of the Capillucas dam.

Figure 7.

Relationship between suspended sediment concentrations (SSC) and discharge for Chavin, Putinza, Huantan and Azucha stations. Data was collected during our fieldwork campaign in 2018. n is the number of samples collected at each station. The resulting rating curves were consequently used for the sediment transport model calibration.

Figure 8.

Calibration of the hydrological model. Comparison between the observed (blue lines) and modelled data (orange lines) for the period 2014-2015.

Figure 9.

Calibration of the sediment transport model. Comparison between the observed and modelled data for the period 2014-2015. The blue lines represent the observed data and the orange ones the output of the model.

Figure 10.

The projected discharge for eight climate change scenarios. The A scenarios involved an equal distribution of the rainfall increase over the rainy season, while the B scenarios involved a precipitation increment only during the rainfall peaks. The rainfall depths are given in bars, and the flow rates in solid lines. The X-axis represents the date, the reversed right Y-axis represents rainfall and the right Y-axis represents discharge.

Figure 11.

Mean discharge during the rainy season for the Putinza gauging station, as a function of the change in precipitation distribution (A and B) and precipitation amount (-17%, 0%, +5%, +8%, +10%, +15%).

Figure 12.

Comparison of the calibration model and projected climate change scenarios. (a) Sediment load (Q_s) at Putinza station; (b) Volume of trapped sediments in the Capillucas storage reservoir. (c) Lifespan of the Capillucas reservoir: timing of reaching the dead and total storages.

Table 1.

Selected efficiency indexes to compare the observed (O_i) and projected (P_i) model outcomes. n is the total number of flood events used for calibration (Krause et al., 2005; Moussa and Chahinian, 2009).

Table 2.

Input data used to build the hydrological (HM) and sediment transport (STM) model.

Table 3.

Accumulative grain size distribution (%) for the upper, middle upper, middle and lower reach of the Cañete River.

Table 4.

Seasonal rainfall changes of two Global Circulation models (GCM) from the Coupled Model Intercomparison Project Phase 5 (CMIP5). Emission scenarios: RCP 2.6 (optimist, high mitigation of gas emissions) and RCP 8.5 (pessimist, highest greenhouse gas emissions). After Fluixá et al. (2018).

Table 5.

Projected rainfall scenarios for the Cañete basin. The change in precipitation rate has been applied to the rainy season (Dec. - Feb.).

Table 6.

Calibration indexes obtained at the calibration sites for the hydrologic model. E: Nash-Nash-Sutcliff, r^2 : Coefficient of determination, d: index of agreement, RVB Relative volume bias and KGE: Kling-Gupta efficiency.

Table 7.

Calibration indexes for the four calibration sites. E: Nash-Nash-Sutcliff, r^2 : Coefficient of determination, d: index of agreement, RVB Relative volume bias, KGE: Kling-Gupta Efficiency; ΔQ_s sediment load difference between modelled and observed data.

Table 8.

Modelled sediment load at Putinza station and modelled amount of trapped sediments at Capillucas dam.

Abstract

Recent changes in global climate, and especially changes in precipitation patterns, may negatively impact on siltation of Andean storage reservoirs, thereby putting at risk the provision of resources to the local population. The extent to which this may happen is poorly understood. We therefore studied the catchment of the Cañete River in the western Peruvian Coastal Range as it plays an important role in the socioeconomic development of the region. It houses the 220MW El Platanal hydroelectric plant and the Capillucas reservoir that provide the surrounding areas with water and energy. We used a hydrological model (HEC-HMS) coupled with a sediment transport model (HEC-RAS) to simulate future changes in river discharge and sediment load. This information was then used to calculate the siltation of the Capillucas storage reservoir. Ten scenarios were developed, a combination of two different precipitation patterns and five different precipitation rates. The precipitation patterns differed in the distribution of the precipitation change during the rainfall season, and the precipitation rates

differed in the extent of change in precipitation amounts. The average sediment load of the Cañete River was estimated at 981 kTon/yr upstream of the Capillucas reservoir and showed that the calculated life span of the Capillucas reservoir is about 17 years. The most pessimistic scenario suggested a reduction in the life span of the reservoir to 7 years and the most optimistic scenario to 31 years. Even under the most optimistic scenario, the life span of the reservoir is shorter than its officially expected functionality of 50 years. As such, our results demonstrated the vulnerability of Andean hydroelectric reservoirs against future climate change.

Highlights

- Hydroelectric reservoirs are highly vulnerable to climate variability.
- An exponential relation exists between precipitation and sediment load
- Changes in precipitation pattern control sediment load of Andean rivers.
- The lifespan of Andean reservoirs may reduce as much as 62% due to silting processes

Captions

Figure 1.

Cañete river basin. Location of the basin within southern Peru, with indication of rural centres, and location of the Capillucas storage dam.

Figure 2.

Physiographic characteristics of the Cañete basin, (a) Lithology map (Navarro Colque, 2016) and (b) Sub-division of the basin in four zones: lower, middle, middle upper and upper sections of the basin (Aybar Camacho and Lavado-Casimiro, 2017).

Figure 3.

Flow diagram of the proposed methodology.

Figure 4.

Representation of basin precipitation-runoff process, adapted from (Arlen, 2000).

Figure 5.

Spatial distribution of meteorological ground stations (rainfall and temperature data) and flow measurement (gauging) stations in Cañete basin.

Figure 6.

Relation of suspended sediment concentration, SSC, and discharge (left side), and rating curve assigned (right side) to Putinza station. The data was collected at Chavin gauging station over the periods 1998-99, 2000 and 2001 before the construction of the Capillucas dam.

Figure 7.

Relationship between suspended sediment concentrations (SSC) and discharge for Chavin, Putinza, Huantan and Azucha stations. Data was collected during our fieldwork campaign in 2018. n is the number of samples collected at each station. The resulting rating curves were consequently used for the sediment transport model calibration.

Figure 8.

Calibration of the hydrological model. Comparison between the observed (blue lines) and modelled data (orange lines) for the period 2014-2015.

Figure 9.

Calibration of the sediment transport model. Comparison between the observed and modelled data for the period 2014-2015. The blue lines represent the observed data and the orange ones the output of the model.

Figure 10.

The projected discharge for eight climate change scenarios. The A scenarios involved an equal distribution of the rainfall increase over the rainy season, while the B scenarios involved a precipitation increment only during the rainfall peaks. The rainfall depths are given in bars, and the flow rates in solid lines. The X-axis represents the date, the reversed right Y-axis represents rainfall and the right Y-axis represents discharge.

Figure 11.

Mean discharge during the rainy season for the Putinza gauging station, as a function of the change in precipitation distribution (A and B) and precipitation amount (-17%, 0%, +5%, +8%, +10%, +15%).

Figure 12.

Comparison of the calibration model and projected climate change scenarios. (a) Sediment load (Qs) at Putinza station; (b) Volume of trapped sediments in the Capillucas storage reservoir. (c) Lifespan of the Capillucas reservoir: timing of reaching the dead and total storages.

Declaration of interests

The authors declare that they have no known competing financial interests or personal relationships that could have appeared to influence the work reported in this paper.

The authors declare the following financial interests/personal relationships which may be considered as potential competing interests:



